Vol. 05, No. 4 (2023) 781-792, doi: 10.24874/PES05.04.020

Proceedings on Engineering Sciences

www.pesjournal.net

# CRITICAL SPEED IN PEDESTRIANS' RELATIVE MOTION REGARDING LIMITED VISIBILITY ZONE FROM DRIVER SEAT

Hristo Uzunov [1]
Silvia Dechkova
Vasil Uzunov

Received 17.04.2023.
Accepted 23.11.2023.
UDC – 656.052.5

Keywords:

*Visibility, Stopping, Automobile, Pedestrian, Movement, Critical Speed*

A B S T R A C T

*Safe driving is related to the choice of speed by automobile drivers according to atmospheric conditions, as well as when driving in zones of both reduced visibility and of limited visibility. Reduced visibility is associated with natural phenomena, such as fog, rain, snow, darkness, etc. Limited visibility is related to objects located on the traffic lane and near it, as well as topography of the area that obstruct the visibility of the driver. This paper outlines a dynamic study of a significant problem in driving connected with limited visibility from the driver's seat due to automobile interior equipment. The research was done implementing experimental and numerical study, obtaining the relative motion of a zone of partially limited visibility from the front left and right car pillars in relation to the trajectory of the pedestrian. At the moment of pedestrian detection, they fall into the danger zone for the car.*



## 1. INTRODUCTION

The distance of visibility for the driver in the overview glass is directly related to the speed of motion of the car center of mass, and this is determined by the so-called danger zone for the car (fig. 1-6), (Zhang & Ma, 2014; Uddin & Ahmed, 2018; Campbell, 1974; Taki et al., 2019). Automobile drivers of a moving car should take into account the speed of the car's center of mass in order to be able to stop in the visible area, in other words, the distance from the moment the driver perceives danger to the final position of rest should be greater than the danger zone for the car. The danger zone for the car is also known as the vehicle total stopping distance, which occurs during an emergency stop while driving (Lyubenov et al., 2019; Lyubenov et al., 2022).

**Figure 1.** Reduced visibility due to fog

Corresponding author: Hristo Uzunov
Email: hvuzunov@gmail.com

**Figure 2.** Reduced visibility due to snowfall

**Figure 3.** Reduced visibility in the hours of darkness

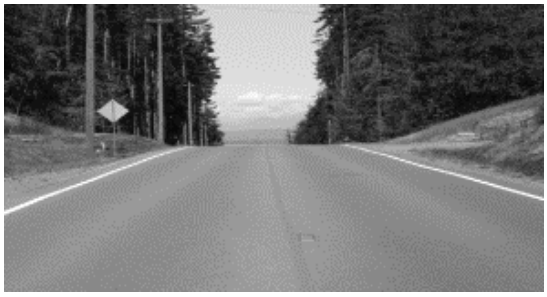

**Figure 4.** Limited visibility due to terrain

**Figure 5.** Limited visibility beyond the bend


**Figure 6.** Limited visibility due to a moving object

The danger zone represents the amount

$$s_o = s_{\text{р}} + s_{\text{сп}} + s_{\text{н}} + s, \qquad (1)$$

where it contains the following elements:
$s_{\text{р}}$ - the distance the vehicle travels during 'driver's reaction time' $t_{\text{р}}$;
$s_{\text{сп}}$ - the distance the vehicle travels during 'brake activation time' $t_{\text{сп}}$;
$s_{\text{н}}$ - the distance the vehicle travels during braking delay rise time from zero to maximum" $t_{\text{н}}$;
$s$ - effective braking distance, which is the distance the vehicle travels during driving with maximum braking delay $t_s$, and during this movement the car leaves skid marks.

The danger zone for the car has the form (Fig. 7):

$$s_o = (t_p + t_{cp} + 0{,}5.t_{\text{н}}).V + \frac{V^2}{2.j}, \qquad (2)$$

where $t_{\text{н}}$ - delay rise time from zero to maximum; $t_{cp}$ - time to actuate the braking system; $t_p$ - driver reaction time; $j$ – deceleration.

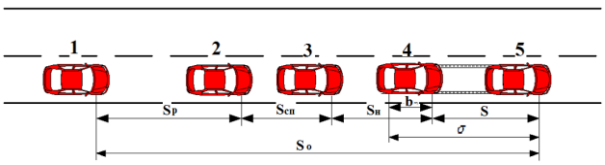


**Figure 7.** Elements of the total stopping distance/danger zone for the car

## 2. INVESTIGATION OF PARTIALLY RESTRICTED VISIBILITY FROM THE DRIVER'S SEAT DUE TO AUTOMOTIVE INTERIOR COMPONENTS

Perception of objects in front and on both sides of the car in their relative motion is essential to car safety (Henderson et al. 2022; Dimitrov et al., 2021; Damyanov, 2020; Saliev & Damyanov, 2022; Jaksch, 1973; Severy et al., 1967).

The characteristic features of the compartment in certain cases serve as an obstacle for the driver to perceive a moving object - a car, a cyclist, a moped rider, a pedestrian. This problem is particularly significant in intersection areas, where the intensity of traffic flows is significant. The front two pillars are of different sizes, designs and constructional features, their location being further forward than the position of the driver's head relative to the car's own coordinate system, invariably connected to the car. When looking aside to the pillar, a cone-shaped zone of limited visibility is featured. (Fig. 8).

In the relative motion between the investigated car and the moving object /pedestrian, motor vehicle/ there is a critical speed for the object under investigation, at

which this moving object falls permanently into the zone of limited visibility. This means that the displacement of the zone of limited visibility coincides with the time of the relative motion of the moving object under study.

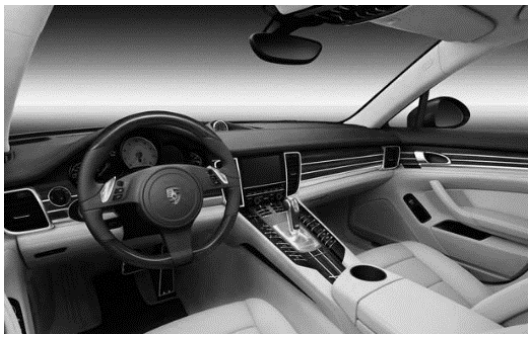

**Figure 8.** Equipment elements and partially limited visibility from the front pilla

A special area of the present study is cars passing through an intersection. In order to ensure unhindered passage through the intersection, the driver should yield the moving vehicles on the right-of-way or the moving pedestrians on the crossing. This means that, in addition to stopping at the stop line or at the level of the border of the intersection, when entering the intersection, moving objects that have the right of way should be perceived.

With a relatively constant driver position in the passenger compartment, the zone of limited visibility is displaced with the moving coordinate system and in accordance with the speed of motion of the car center of mass (Fig. 9).

A study of the areas of limited visibility was carried out for low-end, mid class, luxury cars and SUVs (Fig. 10-14).

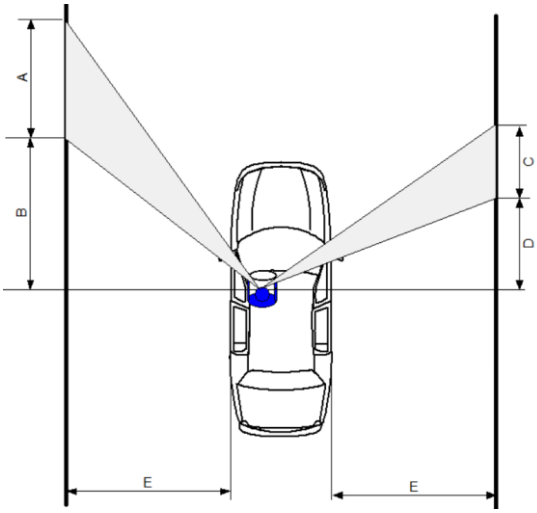


**Figure 9.** Zones of partially limited visibility

Low-end car | Mid class | Luxury car | SUV

**Figure 10.** Areas of restricted visibility for cars

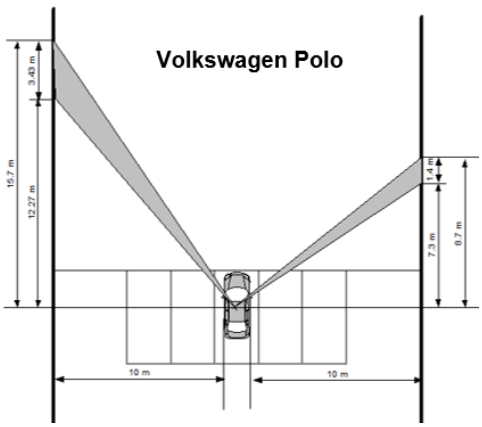


Schematic diagram of geometric dimensions


Photographs of the measurements

**Figure 11.** Volkswagen Polo

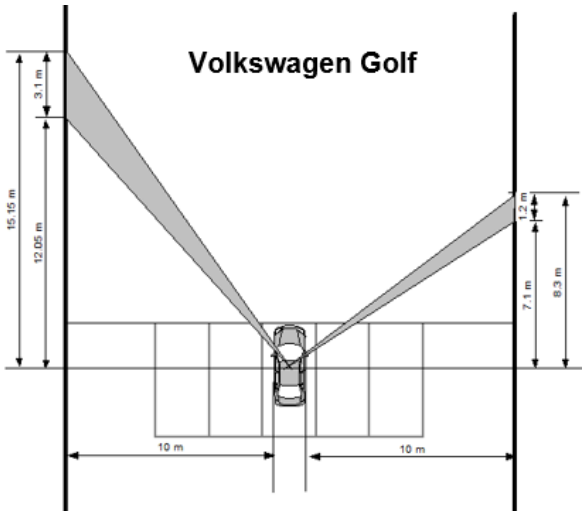



Schematic diagram of geometric dimensions Photographs of the measurements

**Figure 12.** Volkswagen Golf

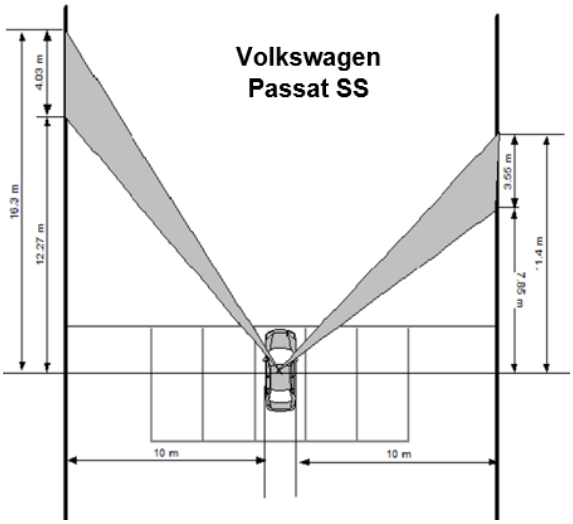


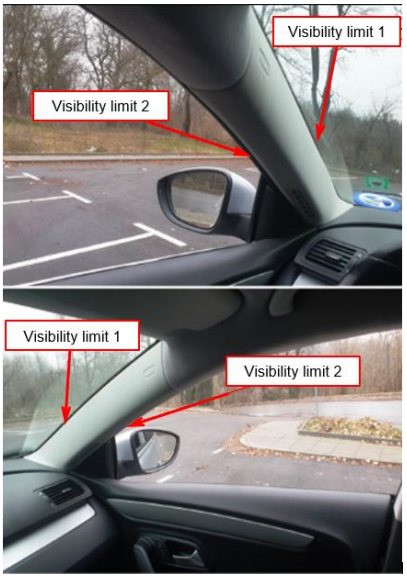


Schematic diagram of geometric dimensions Photographs of the measurements

**Figure 13.** Volkswagen Passat SS

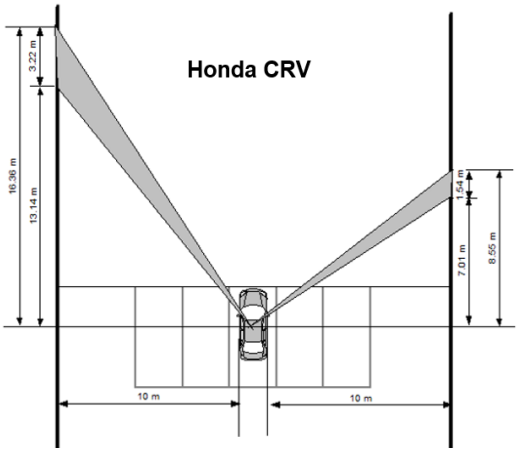



Schematic diagram of geometric dimensions Photographs of the measurements

**Figure 14.** Honda CRV

Zones of limited visibility are especially dangerous when the car is moving straight at an intersection, when maneuvering a left or right turn. For this purpose, a specific analysis of a mid-range car in a right-turn and left-turn intersection was carried out. Specific data on the relative motion of the restricted visibility area was obtained.

*Example 1:* The first experiment is a right turn for a mid-size car moving in the intersection area. A Volkswagen Golf car is positioned at the intersection before the stop line (Fig. 15).

Four cone coloured markers were used to mark individual positions. The measurement is at a displacement step of a mid-range car of 2.5 m. The zones of step-by-step movement of the car are marked with a different color, as follows: 1 - orange, 2 - red, 3 - green, 4 - blue. In the final position, the appearance of a pedestrian in the area visible to the driver is recorded in the windshield visibility.

At the relative displacement of the vehicle and the pedestrian, there is a critical speed of the pedestrian's center of mass, at which he falls permanently into the sector of partially limited visibility and out of the driver's view during the right turn maneuver.


**Figure 15.** Right-turn experiment for a car moving in the intersection area

*Example 2:* The second experiment is a left turn for a car moving in the intersection area. A Volkswagen Golf car is positioned at the intersection before the level of the stop line (Fig. 16).

Four cone coloured markers were used to mark individual positions. The measurement is at a displacement step of a mid-range car of 2.5 m. The zones of step-by-step movement of the car are marked with a different color, as follows: 1 - orange, 2 - red, 3 - green, 4 - blue. In the final position, the possibility of the appearance of a pedestrian in the area visible to the driver in the windshield visibility is taken into account.
At the relative displacement of the vehicle and the pedestrian, there is a critical speed of the pedestrian's center of mass, at which he falls permanently into the sector of partially limited visibility and out of the driver's view during the left turn maneuver.


**Figure 16.** Left turn experiment for a car moving in the intersection area

A dynamic model of the relative motion of the zone of limited visibility of the car and the pedestrian has been developed. Based on this model, it has been determined whether there is a critical impact speed of pedestrian motion, at which the driver could not have perceived him/her earlier.

Macro simulation of vehicle motion in case of loss of lateral stability is observed in an arbitrarily accepted absolute coordinate system $OXYZ$ (Niehoff & Gabler 2006; Brach & Brach, 2011; Stronge, 2000; Dechkova, 2018; Uzunov et al., 2021). To study the car motion, it has been assumed that its own coordinate system $Cx'y'z'$ is movable and permenantly connected to the vehicle center of mass $C$ (Fig. 17). In addition, a permanently connected $Cxyz$ coordinate system is attached to it, parallel to the absolute and translationally movable one.
Coordinates of the vehicle center of mass $C$ $x_c, y_c, z_c$ in the fixed coordinate system are selected for generalized coordinates of the car motion.

Rotational motion of the car is expressed by the Euler transformations and corresponding angles, namely $\psi, \theta$ and $\varphi$. The precession angle of $\psi$, taking into account the rotation around the axis $Cz$; respectively, the angular velocity of $\dot{\psi}$ is obtained; the angle $\theta$ of nutation, taking into account the rotation with respect to the axis $C\rho$, the intersection of the planes $0xy$ and $Cx'y$.

Therefore, the force of gravity $\vec{G}$ will lie on the axis $Oz$. The spatial arrangement model of the car is a plane located on four elastic supports, which are marked by $K_i(i = 1 \div 4)$ (Fig. 18) (Kolev & Kadirova, 2019; 2020).
.

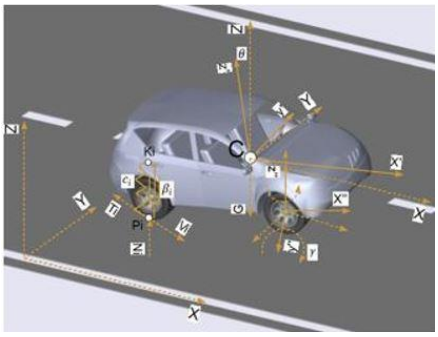

**Figure 17.** Spatial dynamic model of an automobile with elastic suspension

$\vec{F}_i(i = 1 \div 4)$ is elastic force generated by the elasticity of tires and springs; $\vec{N}_i(i = 1 \div 4)$ is normal reaction at the contact point of automobile tires, corresponding to elastic force; $\vec{V}_i(i = 1 \div 4)$ is velocity of the contact point $P_i$ in the plane of the road $0xy$; $\vec{T}_i(i = 1 \div 4)$ is friction force at the contact points that lies in the plane of the road $0xy$; $\vec{R}_i(i = 1 \div 4)$ is resistance force generated by damping elements in suspension; $c_i, \frac{N}{m}(i = 1 \div 4)$ elasticity of suspension, taking into account both coefficient of elasticity of tires and suspension; $b_i, \frac{N \cdot s}{m}(i = 1 \div 4)$ coefficient of linear resistance.

The car motion according to the studies of kinetic energy and generalized forces is defined by six differential equations with six generalized coordinates. These equations are valid if the friction force is in accordance with Coulomb's law and the wheels slide on the ground without rolling. According to (7), the wheels keep a continuous contact with the road (Karapetkov, & Dimitrov, 2022; Karapetkov et al., 2019).

Generalized forces and moments in the right-hand sides of the differential equations (4) are determined by assuming that the absolute coordinate system has a vertical axis of $0z$.

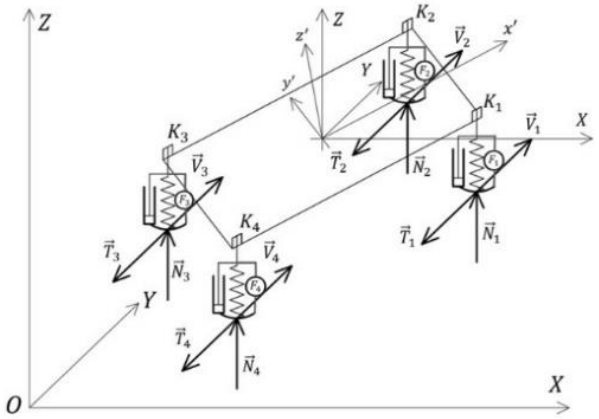


**Figure 18.** Model of the forces acting on a car in its spatial motion, taking into account the elasticity of tires (suspension)

$$m \cdot \ddot{x} = \left[\sum_{i=1}^{4} F_{xi}\right]; \; m \cdot \ddot{y} = \left[\sum_{i=1}^{4} F_{yi}\right]; \; m \cdot \ddot{z} = \left[-G + \sum_{i=1}^{4} N_i - \sum_{i=1}^{4} R_i\right]; \tag{3}$$

$$a_{11} \cdot \ddot{\varphi} + a_{12} \cdot \ddot{\psi} + a_{13} \cdot \ddot{\theta} = \tag{4}$$

$$\begin{Bmatrix} \sum_{i=1}^{4} N_i \cdot \delta_{\varphi i} + \sum_{i=1}^{4} \left(F_{xi} \cdot f_{\varphi_x} + F_{yi} \cdot f_{\varphi_y}\right) - \sum_{i=1}^{4} R_i \cdot \delta_{\varphi i} \\ -b_{11} \cdot \dot{\varphi}^2 - b_{12} \cdot \dot{\psi}^2 - b_{13} \cdot \dot{\theta}^2 - c_{11} \cdot \dot{\varphi} \cdot \dot{\psi} - c_{12} \cdot \dot{\varphi} \cdot \dot{\theta} - c_{13} \cdot \dot{\psi} \cdot \dot{\theta} \end{Bmatrix};$$

$$a_{21} \cdot \ddot{\varphi} + a_{22} \cdot \ddot{\psi} + a_{23} \cdot \ddot{\theta} =$$

$$= \begin{Bmatrix} \sum_{i=1}^{4} \left(F_{xi} \cdot f_{\psi_x} + F_{yi} \cdot f_{\psi_y}\right) - b_{21} \cdot \dot{\varphi}^2 - b_{22} \cdot \dot{\psi}^2 - b_{23} \cdot \dot{\theta}^2 - \\ -c_{21} \cdot \dot{\varphi} \cdot \dot{\psi} - c_{22} \cdot \dot{\varphi} \cdot \dot{\theta} - c_{23} \cdot \dot{\psi} \cdot \dot{\theta} \end{Bmatrix};$$

$$a_{31} \cdot \ddot{\varphi} + a_{32} \cdot \ddot{\psi} + a_{33} \cdot \ddot{\theta} =$$

$$= \begin{Bmatrix} \sum_{i=1}^{4} N_i \cdot \delta_{\theta i} + \sum_{i=i}^{4} \left(F_{xi} \cdot f_{\theta_x} + F_{yi} \cdot f_{\theta_y}\right) - \sum_{i=1}^{4} R_i \cdot \delta_{\theta i} - \\ -b_{31} \cdot \dot{\varphi}^2 - b_{32} \cdot \dot{\psi}^2 - b_{33} \cdot \dot{\theta}^2 - c_{31} \cdot \dot{\varphi} \cdot \dot{\psi} - c_{32} \cdot \dot{\varphi} \cdot \dot{\theta} - c_{33} \cdot \dot{\psi} \cdot \dot{\theta} \end{Bmatrix};$$

$$a_{11} = J_{z'z'};\ a_{12} = -J_{z'z'} \cdot cos\theta - J_{z'x'} \cdot sin\varphi \cdot sin\theta - J_{y'z'} \cdot cos\varphi \cdot sin\theta;$$

$$a_{13} = -J_{z'x'} \cdot cos\varphi + J_{y'z'} \cdot sin\varphi;$$

$$b_{11} = 0;\ b_{12} = \begin{pmatrix} -\frac{1}{2} \cdot sin2\varphi \cdot sin^2\theta \cdot \left(J_{x'x'} + J_{y'y'}\right) + \\ +J_{x'y'} \cdot cos2\varphi \cdot sin^2\theta + \\ +\frac{1}{2} \cdot sin2\theta \cdot \left(J_{z'x'} \cdot cos\varphi - J_{y'z'} \cdot sin\varphi\right) \end{pmatrix};$$

$$b_{13} = \left(\frac{1}{2} \cdot \left(J_{x'x'} - J_{y'y'}\right) \cdot sin2\varphi - J_{x'y'} \cdot cos2\varphi\right);$$

$$c_{11} = 0;\ c_{12} = 0;\ c_{13} = \begin{pmatrix} cos2\varphi \cdot sin\theta \cdot \left(J_{x'x'} + J_{y'y'}\right) - \\ -J_{z'z'} \cdot sin\theta - \\ -2 \cdot \begin{pmatrix} J_{x'y'} \cdot sin2\varphi \cdot sin\theta + \\ +J_{z'x'} \cdot sin\varphi \cdot cos\theta + \\ +J_{y'z'} \cdot cos\varphi \cdot cos\theta \end{pmatrix} \end{pmatrix}$$

$$a_{21} = \left(J_{z'z'} \cdot cos\theta - J_{z'x'} \cdot sin\varphi \cdot sin\theta - J_{y'z'} \cdot cos\varphi \cdot sin\theta\right);$$

$$a_{22} = \begin{pmatrix} J_{x'x'} \cdot sin^2\varphi \cdot sin^2\theta + J_{y'y'} \cdot cos^2\varphi \cdot sin^2\theta + \\ +J_{z'z'} \cdot cos^2\theta - J_{x'y'} \cdot sin2\varphi \cdot sin^2\theta \\ -J_{x'z'} \cdot sin\varphi \cdot sin2\theta - J_{y'z'} \cdot cos\varphi \cdot sin2\theta \end{pmatrix};$$

$$a_{23} = \begin{pmatrix} 0{,}5 \cdot J_{x'x'} \cdot sin2\varphi \cdot sin\theta - \frac{1}{2} \cdot J_{y'y'} \cdot sin2\varphi \cdot sin\theta - \\ -J_{x'y'} \cdot cos2\varphi \cdot sin\theta - J_{z'x'} \cdot cos\varphi \cdot cos\theta + \\ +J_{y'z'} \cdot sin\varphi \cdot cos\theta \end{pmatrix};$$

$$b_{21} = \left(-J_{z'x'} \cdot cos\varphi + J_{y'z'} \cdot sin\varphi\right) \cdot sin\theta;$$

$$b_{22} = 0;\ b_{23} = \begin{pmatrix} \left(0{,}5 \cdot J_{x'x'} \cdot sin2\varphi - \frac{1}{2} \cdot J_{y'y'} \cdot sin2\varphi - \right) \cdot cos\theta + \\ -J_{x'y'} \cdot cos2\varphi \\ +\left(J_{z'x'} \cdot cos\varphi - J_{y'z'} \cdot sin\varphi\right) \cdot sin\theta \end{pmatrix};$$

$$c_{21} = \begin{pmatrix} \left(J_{x'x'} \cdot sin2\varphi - J_{y'y'} \cdot sin2\varphi - 2 \cdot J_{x'y'} \cdot cos2\varphi\right) \cdot sin^2\theta - \\ -\left(J_{z'x'} \cdot cos\varphi - J_{y'z'} \cdot sin\varphi\right) \cdot sin2\theta \end{pmatrix};$$

$$c_{22} = \begin{pmatrix} \left(J_{x'x'} \cdot cos2\varphi - J_{y'y'} \cdot cos2\varphi + 2 \cdot J_{x'y'} \cdot sin2\varphi\right) \cdot sin\theta - \\ -J_{z'z'} \cdot sin\theta \end{pmatrix};$$

$$c_{23} = \begin{pmatrix} \left(J_{x'x'} \cdot sin^2\varphi + J_{y'y'} \cdot cos^2\varphi - J_{x'y'} \cdot sin2\varphi - J_{z'z'}\right) \cdot sin2\theta - \\ -2 \cdot \left(J_{z'x'} \cdot sin\varphi + J_{y'z'} \cdot cos\varphi\right) \cdot cos2\theta \end{pmatrix};$$

$$a_{31} = J_{z'x'} \cdot cos\varphi + J_{y'z'} \cdot sin\varphi;$$

$$a_{32} = \begin{bmatrix} 0{,}5 \cdot \left(J_{x'x'} - J_{y'y'}\right) \cdot sin2\varphi \cdot sin\theta - J_{x'y'} \cdot cos2\varphi \cdot sin\theta - \\ -J_{z'x'} \cdot cos\varphi \cdot cos\theta + J_{y'z'} \cdot sin\varphi \cdot cos\theta \end{bmatrix};$$

$$a_{33} = J_{x'x'} \cdot cos^2\varphi + J_{y'y'} \cdot sin^2\varphi + \frac{1}{2} \cdot J_{x'y'} \cdot sin2\varphi; \;\; b_{31} = J_{z'x'} \cdot sin\varphi + J_{y'z'} \cdot cos\varphi;$$

$$b_{32} = \begin{bmatrix} -\left[0{,}5 \cdot \begin{pmatrix} J_{x'x'} \cdot sin^2\varphi + J_{y'y'} \cdot cos^2\varphi + \\ +J_{z'z'} - J_{x'y'} \cdot sin2\varphi \end{pmatrix}\right] \cdot sin2\theta + \\ +\left(J_{z'x'} \cdot sin\varphi + J_{y'z'} \cdot cos\varphi\right) \cdot cos2\theta \end{bmatrix}; \;\; b_{33} = 0;$$

$$c_{31} = \begin{bmatrix} \left[\left(J_{x'x'} + J_{y'y'}\right) \cdot cos2\varphi + 2 \cdot J_{x'y'} \cdot sin2\varphi + J_{z'z'}\right] \cdot sin\theta + \\ +2 \cdot \left(J_{z'x'} \cdot sin\varphi + J_{y'z'} \cdot cos\varphi\right) \cdot cos\theta \end{bmatrix};$$

$$c_{32} = \left[\left(-J_{x'x'} + J_{y'y'}\right) \cdot sin2\varphi + 2 \cdot J_{x'y'} \cdot cos2\varphi\right]; \; c_{33} = 0$$

We substitute the equations before $\delta_{\varphi i}$ and $\delta_{\theta i}$ using the notation

$$\begin{gathered} \delta_{\varphi i} = [(cos\varphi \cdot sin\theta) \cdot x'_{ki} + (-sin\varphi \cdot sin\theta) \cdot y'_{ki}]; \\ \delta_{\theta i} = [(sin\varphi \cdot cos\theta) \cdot x'_{ki} + +(cos\varphi \cdot cos\theta) \cdot y'_{ki} + (-sin\theta) \cdot z'_{ki}]. \end{gathered} \tag{5}$$

To facilitate notation, substitution has been done, which looks like as follows:

$$f_{\psi xi} = \begin{bmatrix} \begin{pmatrix} -sin\psi \cdot cos\varphi - \\ -cos\psi \cdot sin\varphi \cdot cos\theta \end{pmatrix} \cdot \delta x'_{ki} + \\ + \begin{pmatrix} sin\psi \cdot sin\varphi - \\ -cos\psi \cdot cos\varphi \cdot cos\theta \end{pmatrix} \cdot \delta y'_{ki} + \\ +(-cos\psi \cdot sin\theta) \cdot \delta z'_{ki} \end{bmatrix}; \; f_{\theta xi} = \begin{bmatrix} (sin\theta \cdot sin\psi \cdot sin\varphi) \cdot \delta x'_{ki} + \\ +(sin\theta \cdot sin\psi \cdot cos\varphi) \cdot \delta y'_{ki} + \\ +(-cos\theta \cdot sin\psi) \cdot \delta z'_{ki} \end{bmatrix}$$

$$f_{\varphi yi} = \begin{bmatrix} \begin{pmatrix} -sin\psi \cdot sin\varphi + \\ +cos\psi \cdot sin\varphi \cdot cos\theta \end{pmatrix} \cdot \delta x'_{ki} + \\ + \begin{pmatrix} -sin\psi \cdot cos\varphi - \\ -cos\psi \cdot sin\varphi \cdot cos\theta \end{pmatrix} \cdot \delta y'_{ki} \end{bmatrix}; \; f_{\psi yi} = \begin{bmatrix} \begin{pmatrix} cos\psi \cdot cos\varphi - \\ -sin\psi \cdot sin\varphi \cdot cos\theta \end{pmatrix} \cdot \delta x'_{ki} + \\ + \begin{pmatrix} -cos\psi \cdot sin\varphi - \\ -sin\psi \cdot cos\varphi \cdot cos\theta \end{pmatrix} \cdot \delta y'_{ki} + \\ +(sin\psi \cdot sin\theta) \cdot \delta z'_{ki} \end{bmatrix} \tag{6}$$

$$f_{\theta yi} = \begin{bmatrix} (-cos\psi \cdot sin\varphi \cdot sin\theta) \cdot \delta x'_{ki} + \\ +(-cos\psi \cdot cos\varphi \cdot sin\theta) \cdot \delta y'_{ki} + \\ +(-cos\psi \cdot sin\theta) \cdot \delta z'_{ki} \end{bmatrix}$$

The relative motion of the wheels, the differential(s) and the engine are characterized by a system of four differential equations derived by the Lagrangian method, which has the form of

$$\left[I_\gamma\right] \cdot [\ddot{\gamma}] = \left[M_{\gamma i}\right]; \quad M_{\gamma i} = \{F_{i\tau} \cdot r_i + sign\,(\dot{\gamma}_i) \cdot [M_{di} - f_i \cdot N_i - M_{si}]\} \tag{7}$$

$\vec{F}_{i\tau}$ is tangential component of the tire-road friction force, the positive direction of which is taken backwards, in the more frequent cases of braking or loss of stiffness.

Where $\mu$ is friction coefficient depending on slipping speed on the contact spot; $\vec{r}_i$ – radius of the wheel; $f_i$ – coefficient of rolling friction; $\vec{N}_i$ – normal reaction of the road on wheels; $\left[I_\gamma\right]$ - a square matrix of coefficients in front the actual angular acceleration of the drive wheels, depending on the moment of inertia of the

wheels and the engine; $\dot{\gamma}_i\ /i = 1 \div 4/$ - wheel angular velocity; $[\dot{\gamma}]$ - a matrix-column of the actual angular acceleration of the wheels, two or four of which are propulsive; $M_{di}, M_{si}$ - corresponding engine and brake torque applied to each whee (Uzunov, et al. 2021).

Figure 19 shows the dynamic model of an active suspension system. Figure 20 shows the dynamic diagram of a driving or sliding wheel.

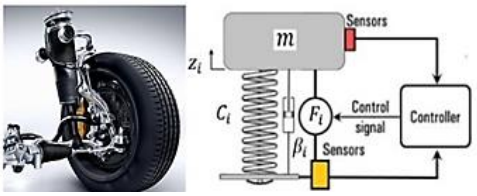


**Figure 19.** Dynamic model of an active suspension system

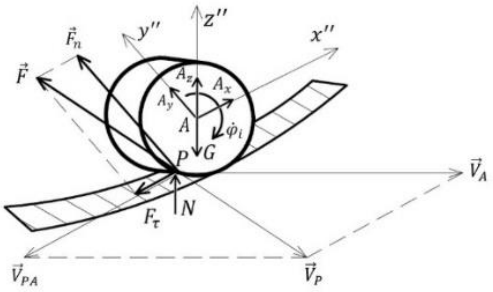


**Figure 20.** Drive wheel diagram

The solutions of the system of differential equations of motion (3) are shown graphically (Fig.21-25).

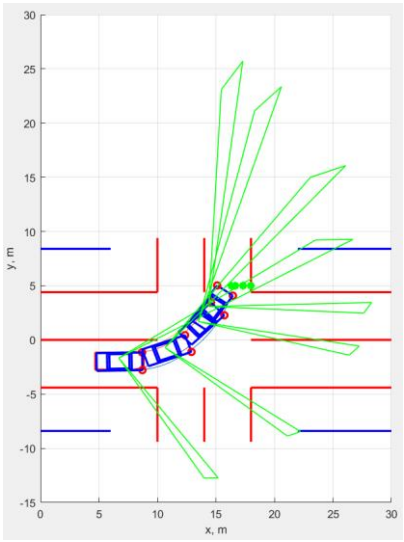


**Figure 21.** Scheme of relative motion between a car and a pedestrian in dynamic aspect

The dynamics of the pedestrian displacement is investigated in steady motion according to the law:

$$V_p = \frac{S_p}{t_p}, \tag{8}$$

where $S_p$ – pedestrian's path; $t_p$ – pedestrian's travel time.

The solution in dynamic aspect is shown by the graphic dependencies:

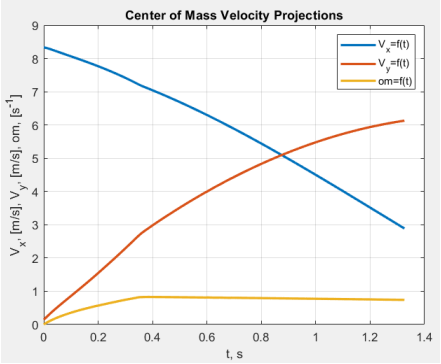


**Figure 22.** Change in center of mass velocity and angular velocity projections about a vertical axis for the car

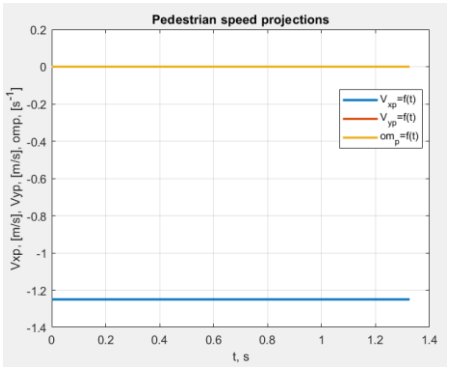


**Figure 23.** Change in the projections of the velocity of the center of mass and angular velocity about a vertical axis for the pedestrian

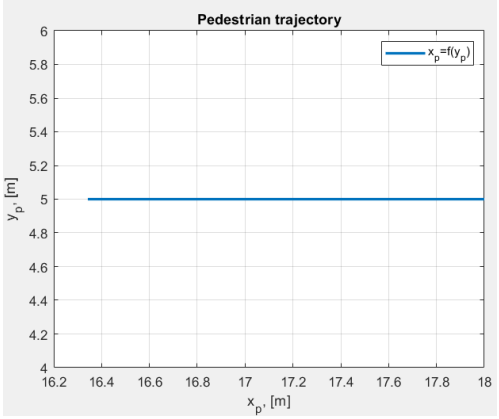


**Figure 24.** Trajectory of the pedestrian's center of mass

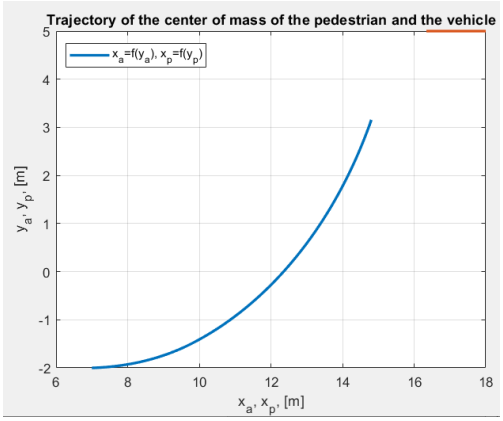


**Figure 25.** Trajectory of the car and the pedestrian's center of mass

The dynamic study thus carried out found that there is a critical speed of motion of the pedestrian's center of mass, which coincides with the relative speed of motion of the zone of limited visibility. When the car driver is able to perceive the pedestrian in the overview of the panoramic windshield, the pedestrian is already in the danger zone for the car.

Analogously, the dynamic study is the same when the car turns right (Fig. 26). In this case, the pedestrian falls into the invisible sector of the front right pillar, right into the blind spot behind the windshield pillar of the vehicle.

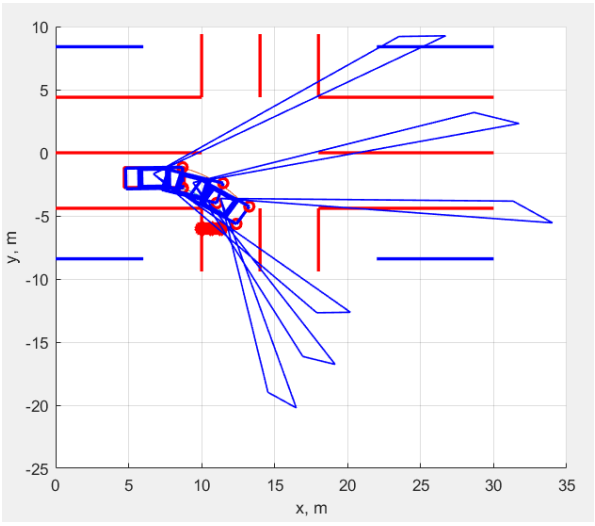


**Figure 26.** Scheme of relative motion between a car and a pedestrian in dynamic aspect

The solution in dynamic aspect is shown by the graphic dependencies (fig. 27-30):

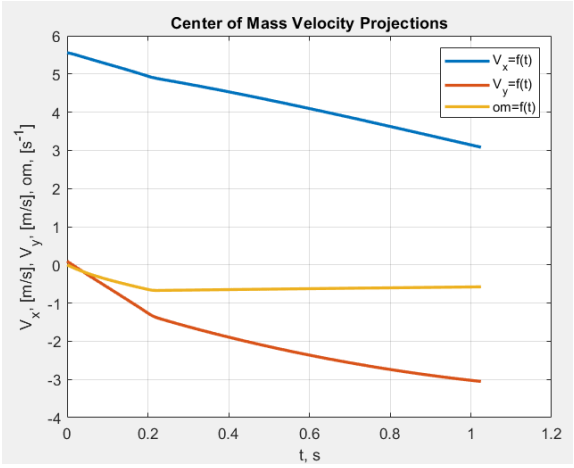


**Figure 27.** Change in center of mass velocity and angular velocity projections about a vertical axis for the car

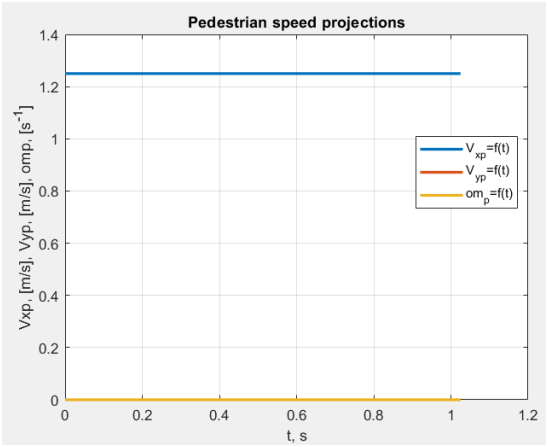


**Figure 28.** Change in center-of-mass velocity and angular velocity projections about a vertical axis for the pedestrian

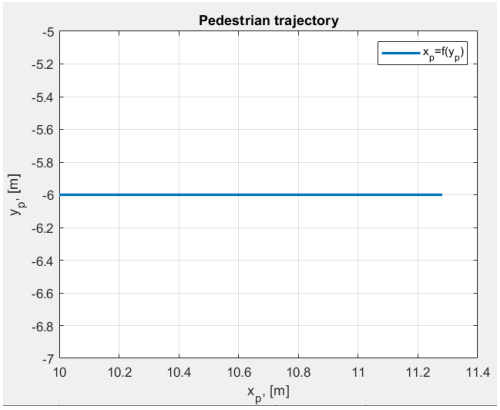


**Figure 29.** Trajectory of the pedestrian's center of mass

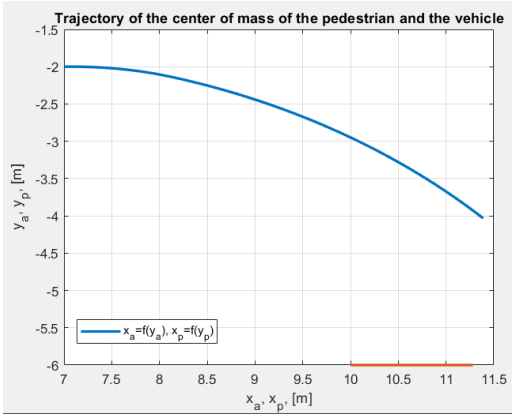


**Figure 30.** Trajectory of the car and the pedestrian's center of mass

## 3. CONCLUSION

1. A dynamic model was developed to study the relative motion between a car and a pedestrian.

2. Visibility in front of the driver depends both on atmospheric conditions (fog, snow, rain, driving at night) and on the equipment of the car – the front windshield pillars.

3. The relative motion between a pedestrian and the zone of limited visibility from the front pillars may cause objects to fall into the danger zone for the car. There is a critical impact speed of relative displacement at which the accident is unavoidable, there is nothing the driver can do to avoid it.

4. The dynamic model presented in this way could be implemented to investigate vehicle accidents in the judicial system on a global scale.

5. To prevent unwanted events, car manufacturers could add an additional mirror determined by the limited visibility sector for the given class car.

**Acknowledgement:** The author/s would like to thank the Research and Development Sector at the Technical University of Sofia for the financial support. organizations should be written in full (optional). Do not include author biographies.

## References:

Brach, R. M., & Brach, M. (2011*). Vehicle Accident Analysis and Reconstruction Methods*, Second Edition. SAE International, 2011. https://doi.org/10.4271/R-397.

Campbell, K. L. (1974). Energy basis for collision severity. *SAE Transactions*, 2114-2126. https://doi.org/10.4271/740565.

Damyanov, I. S. (2020, June). Use of modern software solutions and systems for analysis and reconstruction of road accidents. In *IOP Conference Series. Materials Science and Engineering* (Vol. 878, No. 1). IOP Publishing. https://doi.org/10.1088/1757-899X/878/1/012043.

Dechkova, S. (2018). Creation of multi-mass models in the SolidWorks and Matlab environment for crash identification. *Machine Mechanics*, *119*, 28-32.

Dimitrov, K., Damyanov, I., Saliev, D., & Valkovski, T. (2021, October). Pasture research using aerial photography and photogrammetry. In *2021 29th National Conference with International Participation (TELECOM)* (pp. 121-124). IEEE. https://doi.org/10.1109/TELECOM53156.2021.9659796.

Henderson, R. L., Smith, R. L., Burger, W. J., & Stern, S. D. (1983). Visibility from motor vehicles. *SAE transactions*, 706-730. https://doi.org/10.4271/830564.

Jaksch, F. (1973). Handling and Stability Volvo's Experimental Safety Car. *SAE Transactions*, 2071-2095., https://doi.org/10.4271/730591.

Karapetkov, S., & Dimitrov, L. (2022). An Update on the Momentum 360 Method of Vehicle Impact Reconstruction through 3D Modeling and Computer Simulation. *Symmetry*, *14*(12), 2628. https://doi.org/10.3390/sym14122628.

Karapetkov, S., Dimitrov, L., Uzunov, H., & Dechkova, S. (2019). Identifying vehicle and collision impact by applying the principle of conservation of mechanical energy. *Transport and Telecommunication Journal*, *20*(3), 191-204. https://doi.org/10.2478/ttj-2019-0016.

Kolev, Z. D., & Kadirova, S. Y. (2019, September). Numerical modelling of heat transfer in convector's pipes by ABAQUS. In *IOP Conference Series: Materials Science and Engineering* (Vol. 595, No. 1, p. 012006). IOP Publishing. .https://doi.org/10.1088/1757-899X/595/1/012006.

Kolev, Z., & Kadirova, S. (2020). Numerical modeling of the thermal conduction process in water-air convector's fins. In *E3S Web of Conferences* (Vol. 180). EDP Sciences. https://doi.org/10.1051/e3sconf/202018001009.

Lyubenov, D., Balbuzanov, T., & Dinolov, O. (2022, August). Application of GPS-based information system in studying dynamic properties of vehicles. In *AIP Conference Proceedings* (Vol. 2570, No. 1). AIP Publishing. https://doi.org/10.1063/5.0100026.

Lyubenov, D., Mateev, V., & Kadikyanov, G. (2019, September). An expert system for vehicle accident reconstruction. In *IOP Conference Series: Materials Science and Engineering* (Vol. 614, No. 1, p. 012006). IOP Publishing. https://doi.org/10.1088/1757-899X/614/1/012006.

Niehoff, P., & Gabler, H. C. (2006). The accuracy of WinSmash delta-V estimates: the influence of vehicle type, stiffness, and impact mode. In *Annual proceedings. Association for the Advancement of Automotive Medicine* (Vol. 50, pp. 73-89).

Saliev, D. N., & Damyanov, I. S. (2022, September). Vehicles acceleration rate study for intergreen time of a signal cycle compute. In *AIP Conference Proceedings* (Vol. 2449, No. 1). AIP Publishing. https://doi.org/10.1063/5.0091882.

Severy, D. M., Brink, H. M., & Baird, J. D. (1967). *Collision Performance, LM Safety Car.* pp. 670458. https://doi.org/10.4271/670458.

Stronge, W. J. (2000*). Impact Mechanics.* Cambridge University Press,

Taki, T., Machida, M., & Shimada, R. (2019). Trends of traffic fatalities and DNA analysis in traffic accident investigation. *IATSS research*, *43*(2), 84-89. https://doi.org/10.1016/j.iatssr.2019.05.001.

Uddin, M., & Ahmed, F. (2018). Pedestrian injury severity analysis in motor vehicle crashes in Ohio. *Safety*, *4*(2), 20. https://doi.org/10.3390/safety4020020.

Uzunov, H., Dechkova, S., Dimitrov, K., & Uzunov, V. (2021). Mechanical Mathematical Modeling of a Car Accident Caused by Sudden Mechanical Failure. *Journal of Engineering Science and Technology Review*, 14(4), 61–68. https://doi.org/10.25103/jestr.144.08.

Uzunov, H., Matzinski, P., Dechkova, S., & Dimov, N. (2021). Systems engineering information model of vehicle-pedestrian collisions. *Cybernetics and information technologies*, *21*(1), 151-168. https://doi.org/10.2478/cait-2021-0011.

Zhang, C., & Ma, Y. (2014). Can visibility difference between driver and pedestrian lead to crash?. *Transportation letters*, *6*(4), 165-172. https://doi.org/10.1179/1942787514Y.0000000018.

**Hristo Uzunov**
Technical University of Sofia, Faculty and College – Sliven,
Sliven,
Bulgaria
hvuzunov@gmail.com
ORCID 0000-0003-2229-2828

**Silvia Dechkova**
Technical University of Sofia, Faculty and College – Sliven,
Sliven,
Bulgaria
silviadechkova@gmail.com
ORCID 0000-0002-1784-6956

**Vasil Uzunov**
Technical University of Sofia, Faculty and College – Sliven,
Sliven,
Bulgaria
xavi66@mail.bg